PHYSICAL REVIEW B **78**, 041408(R) (2008)

Topology and electron scattering properties of the electronic interfaces in epitaxial graphene probed by resonant tunneling spectroscopy

H. Yang,[1,2] G. Baffou,[1] A. J. Mayne,[1] G. Comtet,[1] G. Dujardin,[1] and Y. Kuk[2]
[1]*Laboratoire de Photophysique Moléculaire, CNRS, Université Paris Sud, Bâtiment 210, 91405 Orsay, France*
[2]*Department of Physics and Astronomy, Seoul National University, 151-747 Seoul, Republic of Korea*
(Received 16 June 2008; published 28 July 2008)

Z-V scanning tunneling spectroscopy is used to probe the topology and electron scattering properties of the electronic interfaces of monolayer and bilayer graphenes, expitaxially grown on SiC(0001). The dZ/dV spectra validate existing calculations of the interface topology and provide evidence for new electron scattering properties due to changes in the electronic character of the bonding. Two sharp boundaries are observed: between the vacuum and the graphene π state lying above the graphene atom plane and a subsurface barrier between the carbon-rich layer and the bulk SiC.

DOI: 10.1103/PhysRevB.78.041408 PACS number(s): 73.23.−b, 68.37.Ef, 73.20.−r, 81.05.Uw

Graphene is an ultrathin form of graphite made of a sheet of carbon atoms organized in a honeycomb lattice.[1,2] Like many carbon-based nanomaterials such as nanotubes and fullerenes, graphene shows a number of special electronic properties. These include ballistic electron transport,[1,3] superconducting properties,[4] and a manifestation of the Klein paradox.[5] These are due to the two-dimensional (2D) electron gas and the unique electronic structure of graphene.[6] Graphene is a prime candidate for nanoscale electronics applications.[7,8] Atomic scale investigation of the 2D electron transport has revealed remarkable electron confinement, coherence characteristics,[9] and interference effects.[10,11] Graphene can be prepared either as freestanding sheets[1,2] or epitaxially grown on hexagonal SiC surfaces.[12] Current understanding of the electronic and geometric structures of epitaxial graphene on Si-terminated SiC(0001) is provided by recent *ab initio* calculations.[13–15] The carbon-rich layer has a different electronic structure, composed of an undulating graphenelike layer covalently bonded to the SiC substrate with only localized π states.[16] This layer induces a gap and dopes the graphene layers, as seen in several spectroscopy studies.[11,17–21]

Electron interferometry has been used on different surfaces: diamond,[22,23] metals,[24,25] Si(111),[26,27] oxide layers,[28] or thin films.[29,30] In this Rapid Communication, we use resonant tunneling spectroscopy (RTS) to quantitatively investigate the topology and electron scattering properties of the electronic interfaces in graphene. Here, the very precise topological measurements (0.05 Å) of the interfaces validate the calculations of the geometric structures. This method enables buried interfaces to be studied which are not always accessible to conventional techniques and could be applied to molecular layers[31] or graphene on metals.[18,19] RTS is very different because incoming electrons from the scanning tunneling microscope (STM) tip interact with the electronic interfaces at high energy ($\leq$10 eV) with a k vector perpendicular to the graphene layers. We observe strong electron scattering at two sharp interfaces. The top interface, lying 1.7 Å above the top graphene atom plane, is only 0.3 Å wide providing a measure of the topology of the delocalized graphene π electron state. The second scattering interface lies at the top of the bulk SiC below the carbon-rich layer. The graphene and *C*-rich layers are dominated by π bonding, do not play a role in electron scattering, and are effectively transparent. We suggest that the origin of the subsurface barrier is a change in bonding and scattering, which occurs at the first σ-bonded bulk SiC layer.

Here, the graphene layers are grown epitaxially on the silicon face of a highly n-doped 6*H*-SiC(0001) sample by thermal desorption of silicon at high temperature. The STM images were obtained at 300 K in ultrahigh vacuum with an Omicron instrument. *Z-V* spectroscopy curves were obtained by measuring the tip displacement as a function of the applied voltage at a fixed current. STM images and dZ/dV spectra of monolayer and bilayer graphenes are shown in Fig. 1. In the STM image [Fig. 1(a)] of the monolayer all six carbon atoms can be seen while only three carbon atoms of the graphene bilayer are visible [Fig. 1(c)]; here, the two carbon sublattices are no longer equivalent.[11,12,32] Extended bright spots with a 2 nm periodicity are due to a hexagonal $6\sqrt{3}\times 6\sqrt{3}R30$ structure (often called 6×6). This carbon-rich layer lies underneath the graphene layer(s).[13–15]

In *Z-V* spectra the high-voltage bias raises the Fermi level of the tip above the vacuum level of the surface leading to the formation of standing waves in the vacuum between the tip and the surface. These show up as a series of peaks in the derivative dZ/dV. The dZ/dV spectra in Figs. 1(b) and 1(d) are very different for the two surfaces. On the graphene monolayer, the envelope of all the peaks passes through a minimum (node) at 7.5 V [Fig. 1(b)], while the graphene bilayer spectrum contains two nodes at 5.8 and 8.6 V [Fig. 1(d)]. This difference appears to be unique to graphene and provides the opportunity to measure the topology and electron scattering properties of the various electronic interfaces. The presence of a node indicates strong electron reflection at a buried interface; the standing waves in the graphene layer interfere with those in the vacuum. Figures 1(e) and 1(f) show the Si-terminated SiC(0001)3×3 surface and the associated dZ/dV spectrum; there are no nodes.

The dZ/dV spectra are quantitatively modeled by extracting parameters from the curves in Figs. 1(b) and 1(d). These are the position of the first peak, the average full width at half maximum (FWHM) of all the peaks, the number of peaks, the node position(s), and their relative height(s). In

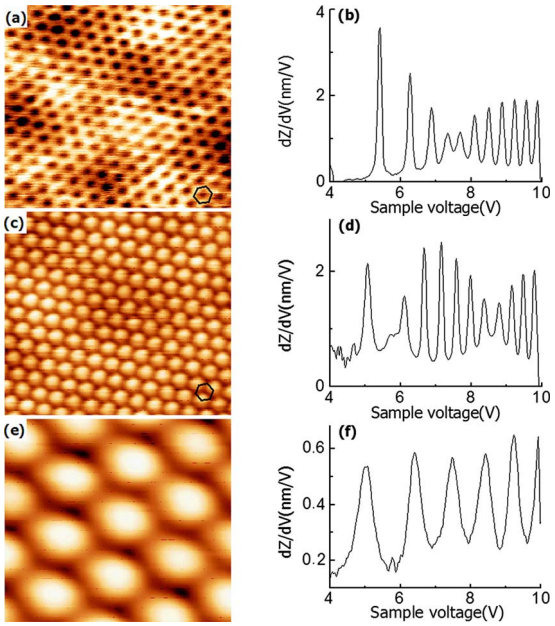

FIG. 1. (Color online) 3×3 nm^2 STM topographic images and corresponding dZ/dV spectra of [(a) and (b)] monolayer graphene, [(c) and (d)] bilayer graphene, and [(e) and (f)] clean SiC(0001)-3×3. The tunnel conditions were (a) −0.05 V, 1.0 nA, (c) −0.05 V, 0.5 nA, and (e) −3.3 V, 0.3 nA. The setpoint current in each dZ/dV spectrum was 0.5 nA.

Fig. 1(b) these values are 5.4 V, 0.14 V, 11, 7.5 V, and 3.25 for the monolayer, and in Fig. 1(d), 5.1 V, 0.26 V, 11, 5.8 V, 8.6 V, and 3.14 for the bilayer. The model simulates the tunnel junction as a trapezoidal barrier determined by the voltage applied to the tip with respect to the surface [Fig. 2(a)]. The Fermi level of the tungsten tip is 8 eV above the conduction-band (CB) minima with a work function of 4.5 V (region 1). In the vacuum (region 2), a slope of 0.143 V/Å is determined, as discussed below, by fitting the experimental

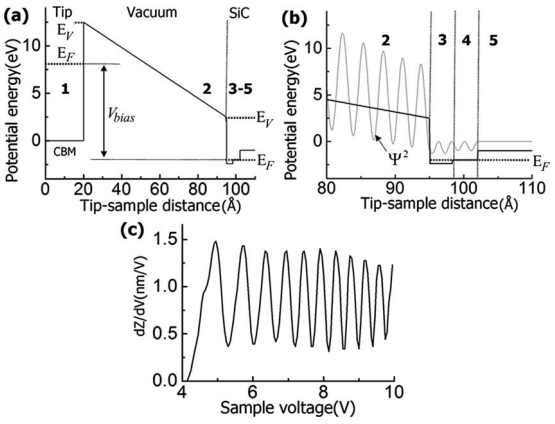

FIG. 2. Trapezoidal potential model with a step potential in the surface region showing: (1) tip, (2) vacuum, (3) graphene, (4) carbon-rich layer, and (5) bulk SiC. (a) All tip and sample energies are with respect to the tip CB minimum. (b) A zoom-in on the vacuum-surface region; the wave form Ψ^2 represents the electron interference. (c) The simulated spectrum shows a series of peaks with no node.

position and the average peak FWHM. As a first attempt [Fig. 2(b)], the trapezoidal potential is combined with the CB minima as the potential energy in sample regions 3–5. The CB minima are often used in potential-energy problems such as semiconducting *p-n* junctions.[5,20,33] The CB minimum of the graphene is placed 400 meV below the Fermi level E_F,[13,14] that of the interface *C*-rich region is at E_F, and that of the bulk SiC 1 eV above E_F [Figs. 2(a) and 2(b)].

Using the CB minima as the potential energy [Fig. 2(a)], the Schrödinger equation is solved numerically using the NDsolve function in MATHEMATICA. The tunnel current from the tip to the sample is determined using specific boundary conditions. The propagative plane-wave solution in the bulk region of the SiC sample (below the electronic interface) is the boundary condition because there is no electron backscattering. The tunneling current is considered to be proportional to the ratio of electron probability ψ^2 between the transmitted wave in the SiC sample and the incident wave in the tip region. In dZ/dV spectroscopy, a fixed current is used. For each calculated spectrum, the slope of the potential barrier in the vacuum junction was kept constant (0.143 V/Å); thus the tip-surface distance increases linearly as the voltage is ramped. Experimentally, the observed linear slope of the *Z-V* curves justifies a constant slope and was determined by fitting the peak position and width in the dZ/dV curves. For each value of V, dZ/dV was obtained by varying V by dV and calculating dZ such that the calculated tunnel current was constant.

As the simulated dZ/dV curve in Fig. 2(c) shows, this model produces a simple progression due to the trapezoidal potential in the vacuum between the tip and the surface. Indeed, no node can be seen, regardless of the thickness between the vacuum-graphene interface and the bulk SiC. The close-up of the electron interferences in the vacuum-surface region in Fig. 2(b) shows that the ratio of the two standing-wave amplitudes for electrons (in the vacuum and in the surface) is too large to induce any node in the dZ/dV spectrum. This model explains the simple progression observed in the SiC(0001)3×3 spectroscopy [Fig. 1(f)]; however, a potential model based solely on the CB minima is insufficient to explain the experimental dZ/dV spectra on graphene. Note that off-normal scattering may occur since the de Broglie wavelength of the electrons is of similar size to the *C*-rich unit cell. However, these electrons play no role in the interferences seen in the dZ/dV spectra. The long tunnel barrier on the tip side acts as a filter, allowing through only electrons with a k vector perpendicular to the surface.[22] The observed interferences are due to scattering normal to the surface only, justifying a one-dimensional (1D) treatment of the problem.

In addition to the outer interface (vacuum graphene), a second potential barrier interface inside the sample must be added [Figs. 3(a) and 3(b)]. The barrier location and the value of the product of the thickness and height (a constant) are determined from two experimental parameters; the locations of the nodes (at 5.8 and 8.6 V) and the interval between them (2.8 V). Using a buried barrier potential strength of 3 eV Å, the experimental dZ/dV curves are compared to the simulations [Figs. 3(c) and 3(d)]. Changing the bilayer thickness shifts both the second node position [Fig. 3(e)] and the

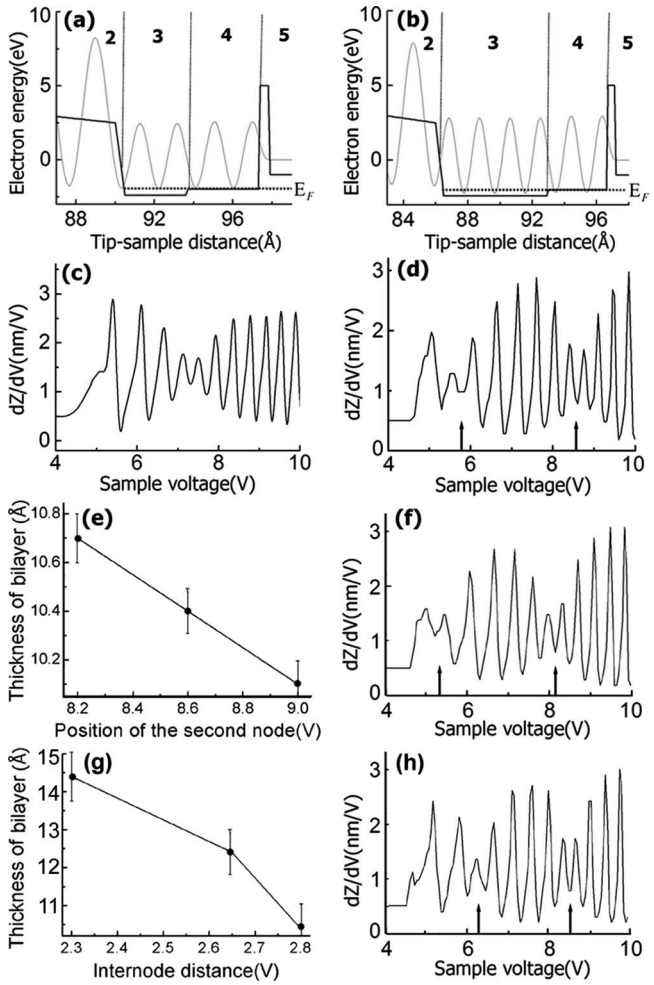

FIG. 3. A potential barrier (6 V × 0.5 Å) is added at the carbon-rich-SiC boundary. A zoom shows the vacuum-surface region of (a) the monolayer and (b) the bilayer, numbered as in Fig. 2. The width of regions 2, 3, and 4 is explained in the text and Fig. 4. The dZ/dV spectra (c) and (d) are the calculated best fit for the monolayer and bilayer, respectively. The calculated bilayer thickness varies with (e) the second node position and (g) the internode distance. The simulated spectra for bilayer thicknesses of (f) 10.7 Å and (h) 14.4 Å poorly fit the experiment in contrast to (c) and (d). The vertical arrows indicate the node positions.

internode distance [Fig. 3(g)]. The simulated spectra for bilayer thicknesses of 10.7 Å [Fig. 3(f)] and 14.4 Å [Fig. 3(h)] poorly fit the experiment; the second node is at 8.2 V in Fig. 3(f) and the internode distance is only 2.3 V in Fig. 3(h). Combined with the monolayer simulation, the best fit is achieved for top to bottom interface separations of 7.05 ± 0.05 and 10.40 ± 0.05 Å for monolayer and bilayer graphene, respectively, as shown in Figs. 3(c) and 3(d). The buried potential width (0.5 Å) is wider than the estimated buckling of the top Si atoms of the SiC bulk.[14] This potential barrier is indispensable since the shift in the CB minimum is not sufficient to create the nodes in the spectra. Furthermore, electron scattering is determined more by the electronic structure and density of states at the interface than the actual atomic positions. Other options, for example, placing the buried barrier closer to the surface between the graphene and

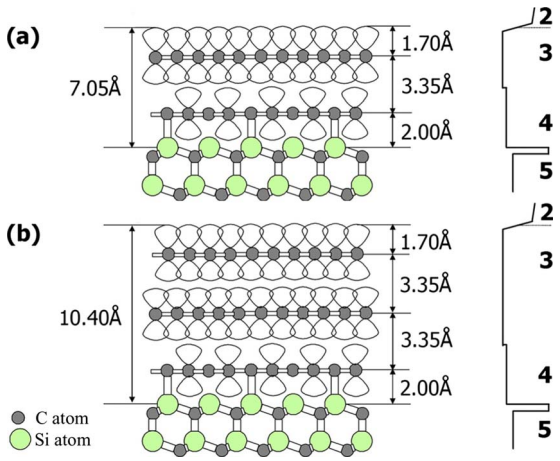

FIG. 4. (Color online) Model of the graphene-SiC interface for the (a) monolayer and (b) bilayer shows schematically regions 2–5: the graphene layer(s), the carbon-rich layer, and the bulk SiC. The π orbitals are shown as lobes and the σ orbitals as bonds joining the atoms. The model potential used to simulate the dZ/dV spectra is projected to the side.

carbon-rich layer, did not work. To fine tune the simulation, we considered a steeply sloped potential drop between regions 2 and 3 in Figs. 3(a) and 3(b) using the observed ratio of the internode peak height to the node peak height. The best fit gave a width of 0.3 ± 0.1 Å, indicating a very sharp boundary between vacuum (region 2) and graphene (region 3). In the simulations, band bending or tip effects were not considered, but the simulated dZ/dV and experimental curves fit well enough to suggest that they do not play an important role.

Figure 4 illustrates the structure of (a) the monolayer and (b) the bilayer with the carbon-rich layer and the bulk SiC, showing the derived interface positions. The difference between the outer and buried electronic scattering interfaces of the bilayer (10.40 ± 0.05 Å) and monolayer (7.05 ± 0.05 Å) is 3.35 ± 0.1 Å, corresponding to the graphene layer thickness. This value is identical to the interplane distance in graphite.[14] Furthermore, we take the calculated interplane distance of 3.35 Å between the *C*-rich layer and the graphene, as well as a bond length of 2.0 Å between the *C*-rich layer and the bulk SiC(0001).[13,14] These results have two important consequences. First, this places the outer scattering potential barrier at the vacuum-graphene interface 1.7 Å above the carbon atoms of the top graphene layer. This outer electronic interface is very sharp (0.3 ± 0.1 Å) and is compatible with a sharp image potential as calculated on graphite.[34] Second, these results demonstrate that the graphene-graphene and graphene-carbon-rich interfaces are transparent to the electrons so that backscattering occurs at the buried interface corresponding to the σ bonded bulk SiC. The density-functional theory (DFT) calculations indicate the amplitude of the buckling of the *C*-rich layer is around 1 Å over the width of the 6×6 unit cell.[13,15] However, no differences were observed in the dZ/dV spectra as a function of the tip position across the surface. This suggests that the buffer layer does not influence the electron scattering; it is effectively transparent and is thus not the origin of the sub-

surface barrier. As we suggest, scattering occurs at the first pure σ-bonded bulk SiC layer. Usually, scattering occurs at insulator-metal interfaces because of the large difference between the energy levels. This is not so in graphene, where the CB minima have similar energies. The carbon layers (graphene and *C* rich) are dominated by π bonding while the bulk SiC is σ bonded.[15,17] This suggests that scattering occurs due to the very different geometries of the electron orbitals.

Electron interferometry, performed by STM *Z-V* spectroscopy, is a unique method for probing the detailed topology and electron scattering properties of the electronic interfaces in epitaxial graphene layers. Monolayers and bilayers of graphene are easily distinguished and very precise information on the position and width of the electronic interfaces is provided. The results show the existence of electronic scattering interfaces 1.7 Å above the graphene layer atoms and at the boundary between the *C*-rich layer and the bulk SiC. However, within the carbon layers, scattering is negligible. The high sensitivity (± 0.05 Å) of this electron interferometry method should allow precise measures of the local variations of an interface position upon intercalation of atoms, molecules, or defects in the graphene layers. These findings are of interest for applications of epitaxial graphene involving electrical contacts, transistor effects, and molecular layer formation, where electronic interfaces play a key role.

H.Y. thanks the France-Korean exchange program for financial support and the opportunity to work at LPPM.

[1] K. S. Novoselov, A. K. Geim, S. V. Morozov, D. Jiang, M. I. Katsnelson, I. V. Grigorieva, S. V. Dubonos, and A. A. Firsov, Nature (London) **438**, 197 (2005).
[2] A. K. Geim and K. S. Novoselov, Nat. Mater. **6**, 183 (2007).
[3] Y. B. Zhang, Y.-W. Tan, H. L. Stromer, and P. Kim, Nature (London) **438**, 201 (2005).
[4] T. E. Weller, M. Ellerby, S. S. Saxena, R. P. Smith, and N. T. Skipper, Nat. Phys. **1**, 39 (2005).
[5] M. I. Katsnelson, K. S. Novoselov, and A. K. Geim, Nat. Phys. **2**, 620 (2006).
[6] A. Bostwick, T. Ohta, T. Seyller, K. Horn, and E. Rotenberg, Nat. Phys. **3**, 36 (2007).
[7] C. Berger *et al.*, J. Phys. Chem. B **108**, 19912 (2004).
[8] J. Hass, R. Feng, T. Li, X. Li, Z. Song, W. A. de Heer, P. N. First, E. H. Conrad, C. A. Jeffrey, and C. Berger, Appl. Phys. Lett. **89**, 143106 (2006).
[9] C. Berger *et al.*, Science **312**, 1191 (2006).
[10] P. Mallet, F. Varchon, C. Naud, L. Magaud, C. Berger, and J.-Y. Veuillen, Phys. Rev. B **76**, 041403(R) (2007).
[11] G. M. Rutter, J. N. Crain, N. P. Guisinger, T. Li, P. N. First, and J. A. Stroscio, Science **317**, 219 (2007).
[12] I. Forbeaux, J.-M. Themlin, and J.-M. Debever, Phys. Rev. B **58**, 16396 (1998).
[13] A. Mattausch and O. Pankratov, Phys. Rev. Lett. **99**, 076802 (2007).
[14] F. Varchon *et al.*, Phys. Rev. Lett. **99**, 126805 (2007).
[15] S. Kim, J. Ihm, H.-J. Choi, and Y.-W. Son, Phys. Rev. Lett. **100**, 176802 (2008).
[16] K. V. Emtsev, T. Seyller, F. Speck, L. Ley, P. Stojanov, J. D. Riley, and R. C. G. Leckey, Mater. Sci. Forum **556**, 525 (2007).
[17] S. Y. Zhou, G.-H. Gweon, A. V. Fedorov, P. N. First, W. A. de Heer, D.-H. Lee, F. Guinea, A. H. Castro Neto, and A. Lanzara, Nat. Mater. **6**, 770 (2007).
[18] S. Marchini, S. Günther, and J. Wintterlin, Phys. Rev. B **76**, 075429 (2007).
[19] A. L. Vázquez de Parga, F. Calleja, B. Borca, M. C. G. Passeggi, J. J. Hinarejos, F. Guinea, and R. Miranda, Phys. Rev. Lett. **100**, 056807 (2008).
[20] T. Ohta, A. Bostwick, T. Seyller, K. Horn, and E. Rotenberg, Science **313**, 951 (2006).
[21] V. W. Brar, Y. Zhang, Y. Yayon, T. Ohta, J. L. McChesney, A. Bostwick, E. Rotenberg, K. Horn, and M. F. Crommie, Appl. Phys. Lett. **91**, 122102 (2007).
[22] K. Bobrov, A. J. Mayne, and G. Dujardin, Nature (London) **413**, 616 (2001).
[23] K. Bobrov, L. Soukiassian, A. J. Mayne, G. Dujardin, and A. Hoffman, Phys. Rev. B **66**, 195403 (2002).
[24] R. S. Becker, J. A. Golovchenko, and B. S. Swartzentruber, Phys. Rev. Lett. **55**, 987 (1985).
[25] J. I. Pascual, C. Corriol, G. Ceballos, I. Aldazabal, H.-P. Rust, K. Horn, J. M. Pitarke, P. M. Echenique, and A. Arnau, Phys. Rev. B **75**, 165326 (2007).
[26] J. A. Kubby, Y. R. Wang, and W. J. Greene, Phys. Rev. Lett. **65**, 2165 (1990).
[27] J. A. Kubby, Y. R. Wang, and W. J. Greene, Phys. Rev. B **43**, 9346 (1991).
[28] K. Xue, H. P. Ho, J. B. Xu, and R. Z. Wang, Appl. Phys. Lett. **90**, 182108 (2007).
[29] W. B. Su, S. M. Lu, C. L. Lin, H. T. Shih, C. L. Jiang, C. S. Chang, and T. T. Tsong, Phys. Rev. B **75**, 195406 (2007).
[30] H. Liu, J. Yan, H. Zhao, S. Gao, and D. Chen, Phys. Rev. B **76**, 113403 (2007).
[31] L. G. Kaake, Y. Zou, M. J. Panzer, C. D. Frisbie, and X.-Y. Zhu, J. Am. Chem. Soc. **129**, 7824 (2007).
[32] S. Hembacher, F. J. Giessibl, J. Mannhart, and C. F. Quate, Proc. Natl. Acad. Sci. U.S.A. **100**, 12539 (2003).
[33] M. V. Fistul and K. B. Efetov, Phys. Rev. Lett. **98**, 256803 (2007).
[34] J. B. Neaton, M. S. Hybertsen, and S. G. Louie, Phys. Rev. Lett. **97**, 216405 (2006).